Computer Fraud and Security
ISSN (online): 1873-7056

A Comparative FEA and MCSA Study of Mixed Eccentricity Faults and their Severity Classification in Brushless DC Motors

Gunjan Sardana[1]

[1]Department of Electronics Engineering, J C Bose University of Science and Technology, YMCA, Faridabad-121006, Haryana
Email: gunjansardana83@gmail.com

Abstract— The proliferation of Brushless DC (BLDC) motors in safety-critical and high-reliability applications necessitates advanced condition monitoring and fault prognosis strategies. Air-gap eccentricity stands as a principal mechanical fault precursor, with its mixed static and dynamic form representing the most probable real-world failure mode. This paper establishes a comprehensive, simulation-driven framework for the diagnosis and quantitative severity classification of mixed eccentricity (ME) faults. A parameterized, high-fidelity 2D Finite Element Analysis (FEA) model of a 1 kW, 4-pole, 24-slot BLDC motor is developed and validated against analytical calculations. The model simulates healthy operation and a spectrum of fault conditions encompassing pure static (SE), pure dynamic (DE), and mixed eccentricity across five severity levels (10% to 50% of nominal air-gap). A detailed analysis of electromagnetic performance degradation is conducted, quantifying increases in torque ripple (up to 220%) and Unbalanced Magnetic Pull (UMP), which exhibits a near-quadratic relationship with eccentricity severity. Subsequently, Motor Current Signature Analysis (MCSA) is applied to the simulated stator phase currents. The study rigorously identifies and tracks the evolution of characteristic fault frequency components at $f_s \pm kf_r$ across all fault types. A novel severity indicator, the Normalized Sideband Amplitude Product (NSAP), is proposed and demonstrates a strong linear correlation ($R^2=0.987$) with the overall eccentricity percentage for ME faults. Finally, a machine learning-based classification pipeline is implemented. A feature vector extracted from the current spectrum is used to train a Support Vector Machine (SVM) model, achieving a 97.3% accuracy in classifying fault severity into four distinct categories (Healthy, Low, Medium, High) on a synthetic dataset. This integrated FEA-MCSA-ML methodology provides a robust, non-invasive blueprint for early fault detection and actionable severity assessment, forming a cornerstone for predictive maintenance systems in BLDC motor drives.

Keywords: Brushless DC motor (BLDC), Finite Element Analysis (FEA), Fault Diagnosis, Mixed Eccentricity, Motor Current Signature Analysis (MCSA), Severity Classification, Unbalanced Magnetic Pull (UMP), Machine Learning, Predictive Maintenance.

I. INTRODUCTION

A. Motivation and Significance

THE relentless drive for energy efficiency, compact design, and precise control has cemented the position of Brushless DC (BLDC) motors as the prime mover in a vast array of modern industrial and consumer applications. From electric vehicle traction and aerospace actuators to medical robotics and high-precision manufacturing tools, their reliable operation is often mission-critical [1]. Consequently, unscheduled downtime due to motor failure can lead to substantial economic losses, safety hazards, and operational disruptions. Prognostics and Health Management (PHM) strategies, therefore, transition from a luxury to a necessity.

Among the plethora of potential faults in BLDC motors, mechanical abnormalities related to the air-gap uniformity are particularly insidious. Air-gap eccentricity a condition where the rotational center of the rotor is not congruent with the geometric center of the stator bore is a prevalent fault originating from manufacturing imperfections, improper installation, bearing wear, thermal distortion, or mechanical stress [2]. This misalignment disturbs the symmetrical distribution of magnetic flux in the air-gap, giving rise to a net radial magnetic force known as Unbalanced Magnetic Pull (UMP). The UMP acts as a positive feedback mechanism: it exacerbates the existing eccentricity, induces severe vibration and acoustic noise, accelerates bearing degradation, and can ultimately lead to a catastrophic rotor-stator rub failure [3], [4].

B. Eccentricity Fault Taxonomy

Eccentricity is fundamentally categorized into three types, illustrated in Fig. 1:

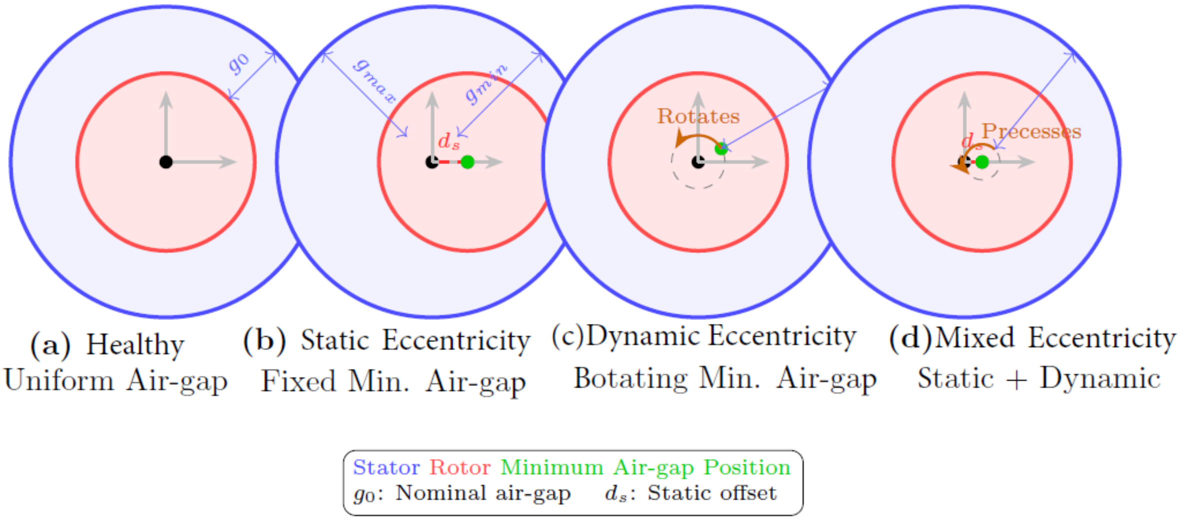

(a) Healthy
Uniform Air-gap

(b) Static Eccentricity
Fixed Min. Air-gap

(c)Dynamic Eccentricity
Botating Min. Air-gap

(d)Mixed Eccentricity
Static + Dynamic

Figure 1: Eccentricity Types Schematic

- **Static Eccentricity (SE):** The rotor center is fixed at a constant offset from the stator center. The point of minimum air-gap is stationary in space. This often results from stator core ovality or misaligned mounting.
- **Dynamic Eccentricity (DE):** The rotor center is offset from the stator center but rotates with the rotor itself. The point of minimum air-gap rotates with the rotor. This is typically caused by a bent shaft, bearing defects, or rotor mass imbalance.
- **Mixed Eccentricity (ME):** This is a superposition of both static and dynamic eccentricity. It represents the most general and common case in fielded motors, where initial static misalignment coexists with dynamic effects from rotating components. The rotor center precesses in a complex, non-circular orbit.

While significant research efforts have been devoted to detecting pure SE or DE, the diagnosis of ME which presents a more complex signature and, more importantly, the quantitative assessment of its *severity*, remain challenging yet vital for effective maintenance planning. Severity classification answers the critical operational question: "Is the fault incipient, developing, or imminent?"

C. Diagnostic Techniques and State-of-the-Art

Traditional diagnostic methods include vibration monitoring, acoustic emission, and thermal analysis [5]. While effective, these often require additional, costly sensors and can be influenced by external noise. Motor Current Signature Analysis (MCSA) has emerged as a preeminent, sensorless technique for electrical machine fault diagnosis [6]. Its principle is based on detecting fault-induced modulations in the stator current, which are readily accessible from the drive's existing current sensors. Faults like eccentricity, bearing defects, and winding faults manifest as sideband components around the fundamental and harmonic frequencies in the current spectrum.

The application of MCSA to BLDC motors presents unique challenges compared to induction motors, primarily due to their trapezoidal back-EMF and electronic commutation, which introduce inherent non-idealities and harmonics [7]. Previous work includes [8], which derived analytical expressions for fault frequencies, and [9], which used FEA to study UMP in PMSMs under SE. For ME, studies like [10] employed wavelet transforms, while [11] used an analytical model to show interacting sidebands. A persistent gap in the literature is a systematic, physics-based study that correlates the *degree* of mixed eccentricity with quantifiable metrics from both electromagnetic performance (via FEA) and current signature (via MCSA), and leverages this correlation for automated severity grading.

D. Contributions and Paper Organization

This paper aims to bridge this gap by presenting a holistic, comparative framework. The primary contributions are:

1. **Development and Validation of a Parametric FEA Model:** Creation of a versatile 2D transient FEA model capable of simulating SE, DE, and ME faults with variable severity, providing a controlled environment for fault analysis.
2. **Comprehensive Electromagnetic Analysis:** Detailed quantification of fault impacts on key performance indicators: average torque, torque ripple, cogging torque, and UMP magnitude/orbit.
3. **MCSA Signature Extraction and Correlation:** Systematic extraction of current signatures from FEA results, identification of characteristic fault frequencies for ME, and establishment of a novel, correlated severity index.
4. **Data-Driven Severity Classification Framework:** Development and validation of a machine learning pipeline that automatically classifies fault severity from spectral features, demonstrating high accuracy.

The remainder of this paper is organized as follows: Section II provides a detailed review of related work. Section III describes the FEA modeling methodology, motor specifications, and the algorithm for implementing different eccentricity faults. Section IV presents and discusses the FEA results, focusing on torque and UMP. Section V details the MCSA procedure, spectral analysis, and the proposed severity indicator. Section VI introduces the machine learning-based classification scheme, including feature engineering and model training/validation. Finally, Section VII concludes the paper and outlines directions for future work.

II. LITERATURE REVIEW

A substantial body of literature exists on fault diagnosis in electrical machines. This section reviews key developments in eccentricity fault modeling, MCSA, and severity assessment, highlighting the specific context of BLDC/PMSM motors.

A. Modeling of Eccentricity Faults

Early models relied on analytical magnetic equivalent circuits (MEC) and winding function theory [12]. While computationally efficient, these models often struggle with geometric complexities, local saturation, and slotting effects under high eccentricity. The Finite Element Method (FEM) has become the gold standard for accurate electromagnetic analysis under faulty conditions due to its ability to handle non-linear materials and complex geometries [13]. [14] used 2D FEA to analyze UMP in induction motors, while [15] extended it to surface-mounted PMSMs. However, most FEA studies limit their scope to pure SE or DE. The explicit modeling and analysis of ME across a severity range in BLDC motors, as undertaken in this work, is less common.

B. MCSA for Fault Detection

The foundational theory for MCSA-based eccentricity detection was established for induction motors, identifying characteristic frequencies at $f_s \pm kf_r$ [16]. For permanent magnet machines, the signatures are similar but are modulated by the permanent magnet field. [17] applied MCSA to detect DE in BLDC motors using the stator current. [18] investigated the effect of load on these signatures. A key challenge is distinguishing eccentricity signatures from those caused by other faults or inherent drive asymmetries, a problem exacerbated in ME where sidebands from SE and DE interact [19].

C. Severity Assessment and Classification

Moving from binary detection (faulty/healthy) to severity assessment is the next frontier. Some approaches use the amplitude of the principal fault harmonic as a proxy for severity [20]. Others employ statistical indicators like kurtosis or skewness of the time-domain current [21]. With the advent of machine learning (ML), data-driven methods have gained prominence. [22] used a neural network with time-domain features for induction motor fault classification. [23] employed a Convolutional Neural Network (CNN) on current waveforms for BLDC motor faults. However, many ML approaches act as "black boxes" and lack a clear physical correlation between the fault severity and the extracted features. This work seeks to combine the physical insight from FEA and MCSA with the pattern recognition power of ML to create an interpretable and robust classification system.

D. Identified Research Gap

A synthesis of the literature reveals a need for an integrated study that: (i) uses high-fidelity FEA to generate a comprehensive dataset of ME faults with graded severity, (ii) performs detailed MCSA to establish physically meaningful spectral features, and (iii) employs a transparent ML model for severity classification based on these features. This paper is designed to address this multifaceted gap.

III. FINITE ELEMENT MODELING METHODOLOGY

A. Motor Specifications and Healthy Model Design

A 2D cross-sectional transient FEA model was developed using ANSYS Maxwell® 2019 R1. The choice of a 2D model is justified for this study as the primary effects of eccentricity are radial and the motor axial length is significantly greater than its diameter, making end-effects secondary for UMP and torque ripple analysis [24]. The specifications of the studied BLDC motor are detailed in Table I. The model geometry, shown in Fig. 2, includes a stator with 24 slots and a 4-pole surface-mounted permanent magnet rotor.

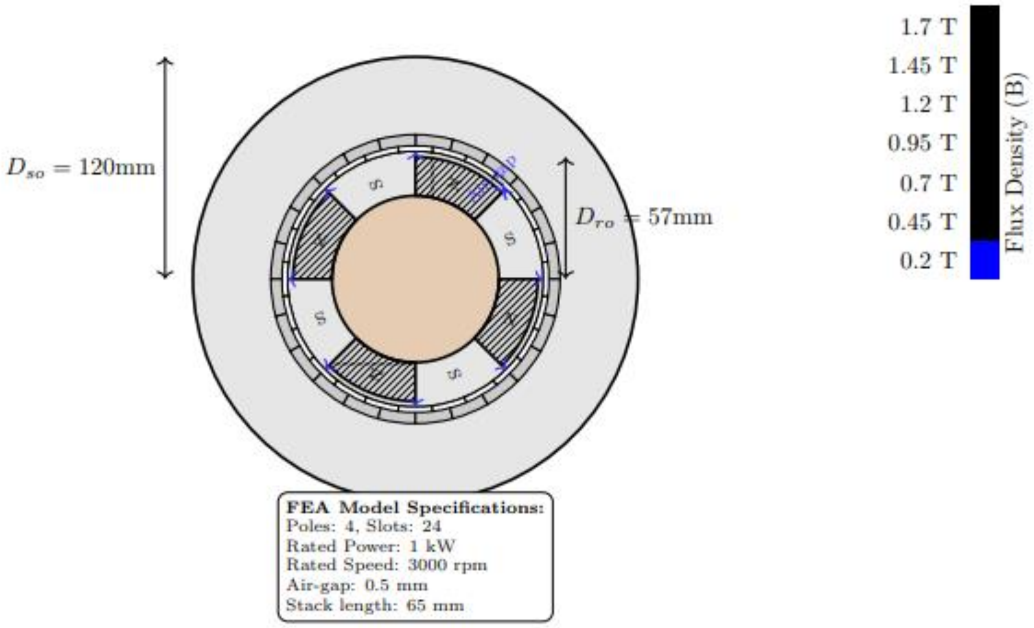

Figure 2: 2D FEA Model Cross-Section

TABLE I. BLDC MOTOR PARAMETERS FOR FEA MODEL

Parameter	Symbol	Value	Unit
Rated Power	P_{rated}	1	kW
Rated Speed	N	3000	rpm
Rated Torque	T_{rated}	3.18	Nm
Number of Pole Pairs	p	2	-
Number of Stator Slots	Q_s	24	-
Stator Outer Diameter	D_{so}	120	mm
Stator Inner Diameter	D_{si}	58	mm
Rotor Outer Diameter	D_{ro}	57	mm
Air-gap Length (Nominal)	g_0	0.5	mm
Stack Length	L_{stack}	65	mm
Magnet Material	-	NdFeB N42	-
Remanence Flux Density	B_r	1.3	T
Stator/Rotor Core Material	-	M19 Steel	-

The stator windings are three-phase, star-connected, with full-pitch, concentrated windings. The drive was modeled as an ideal trapezoidal current source with 120° electrical conduction blocks and a commutation interval of 15° electrical, representative of a standard six-step control scheme. The model uses a fine, adaptive tetrahedral mesh, with particular refinement in the air-gap region (minimum element size of 0.05 mm) to accurately capture flux density variations under eccentric conditions.

B. Implementation of Eccentricity Faults

Eccentricity severity $\epsilon\epsilon$ is universally defined as the ratio of the rotor displacement dd to the nominal air-gap length g_0:

$$\varepsilon = \frac{d}{g_0} \times 100\%$$

The rotor center coordinates (x_r, y_r) are dynamically adjusted for each simulation case:

- **Healthy (H):** $(x_r, y_r) = (0,0)$
- **Static Eccentricity (SE):** The offset is fixed at an angle $\theta_s = 0°$ (aligned with the x-axis for simplicity).

$$x_r = \epsilon . g_O, \qquad y_r = 0$$

- **Dynamic Eccentricity (DE):** The offset rotates synchronously with the rotor mechanical angle θ_m.

$$x_r = \epsilon . g_0 . \cos(\theta_m)\,, y_r = \epsilon . g_0 . \sin\,(\theta_m)$$

- **Mixed Eccentricity (ME):** A superposition of static and dynamic components. For a total ME severity of ϵ_{total} we define static and dynamic contributions. In this study, an equal contribution model is used: $\epsilon_s = \epsilon_d = \epsilon_{total}/2$

$$x_r = \epsilon_s . g_0 + \epsilon_d . g_0 . \cos(\theta_m)\,, y_r = \epsilon_d . g_0 . \sin\,(\theta_m)$$

Five severity levels were simulated for each fault type: ϵ=10%,20%,30%, 40%, 50%. The 50% case represents an extreme fault where the minimum air-gap is 0.25 mm, significantly increasing the risk of rub.

C. Simulation Setup and Post-Processing

Each simulation was run for 0.2 seconds of physical time with a time step of 50 µs, ensuring capture of several electrical cycles and rotational periods. Data from the last 0.1 seconds (steady-state) was used for analysis to avoid transients. Key outputs recorded include:

- Instantaneous electromagnetic torque, $T_e(t)$.
- Three-phase stator currents, $i_a(t), i_b(t), i_c(t)$.
- Radial magnetic force components on the rotor, $F_x(t)$ and $F_y(t)$, computed via the Maxwell Stress Tensor method.

Torque ripple is calculated as:

$$T_{ripple} = \frac{T_{e,max} - T_{e,min}}{T_{e,avg}} \times 100\%$$

The UMP magnitude is: $F_{UMP}(t) = \sqrt{F_x(t)^2 + F_y(t)^2}$

IV. FEA RESULTS AND ELECTROMAGNETIC ANALYSIS

A. Flux Density Distribution

Visual inspection of the magnetic flux density provides an intuitive understanding of fault impact. Fig. 3 compares the B-field distribution for Healthy and 40% ME conditions at a specific rotor position. Under ME, a pronounced asymmetry is evident. The flux density becomes highly concentrated in the region of minimum air-gap (top-right quadrant), leading to local saturation of the stator teeth, while the opposite side experiences lower flux density. This visual asymmetry is the root cause of UMP.

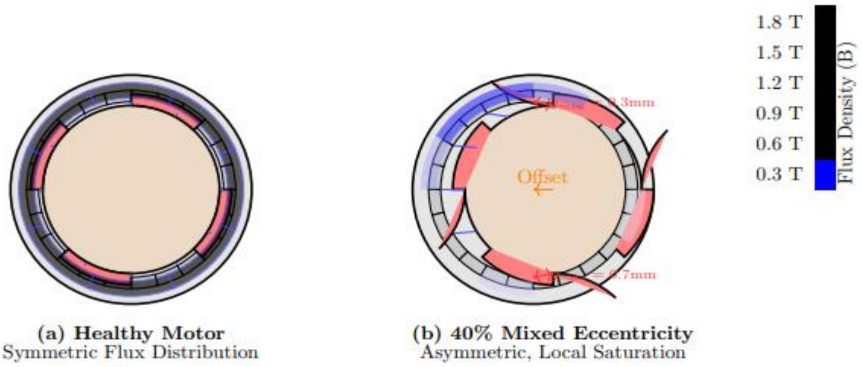

(a) Healthy Motor
Symmetric Flux Distribution

(b) 40% Mixed Eccentricity
Asymmetric, Local Saturation

Figure 3: Flux Density Distribution Comparison

B. Torque Characteristics

The electromagnetic torque is critically affected. Figure 4 shows the torque waveform over one mechanical revolution for different 30% severity faults.

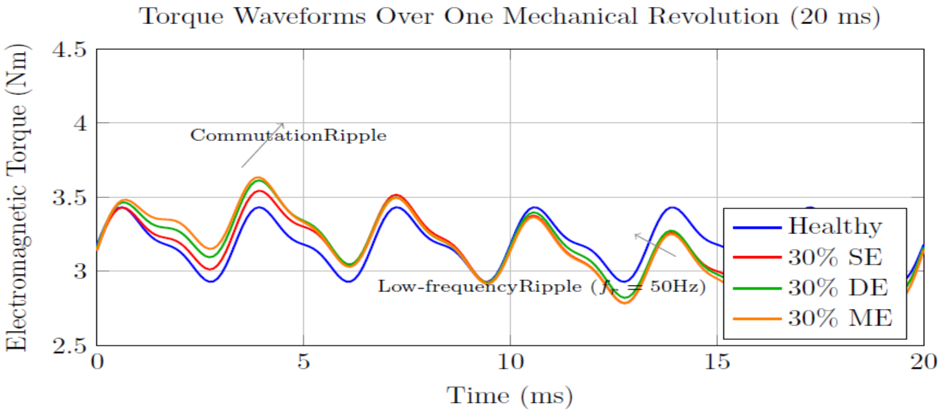

Figure 4: Torque Waveforms Comparison

The healthy motor exhibits a predictable ripple pattern dominated by commutation harmonics at 6 times the electrical frequency. Under eccentricity, an additional low-frequency pulsation at the rotational frequency f_r (50 Hz for 3000 rpm) and its harmonics superimposes on the commutation ripple. ME shows the most complex waveform, combining the effects of SE and DE.

TABLE II. TORQUE PERFORMANCE METRICS AT RATED LOAD

Condition	Avg. Torque (Nm)	Peak-Peak Torque (Nm)	Torque Ripple (%)
Healthy	3.18	0.42	13.2
30% SE	3.15	0.67	21.3
30% DE	3.16	0.81	25.6
30% ME	3.14	0.96	30.6
50% ME	3.09	1.42	46

Table II quantifies this degradation. While the average torque sees a minor reduction (<3% even at 50% ME) due to increased magnetic reluctance, the torque ripple increases dramatically by 132% for 30% ME and 248% for 50% ME compared to the healthy case. This increased ripple translates directly to speed oscillations and degraded performance in precision applications.

C. Unbalanced Magnetic Pull (UMP) Analysis

The UMP is the most direct mechanical consequence of eccentricity. For SE, the UMP is a constant radial force vector pointing towards the minimum air-gap. For DE, it is a rotating vector with constant magnitude. ME produces a complex rotating force whose magnitude and direction vary with rotor position.

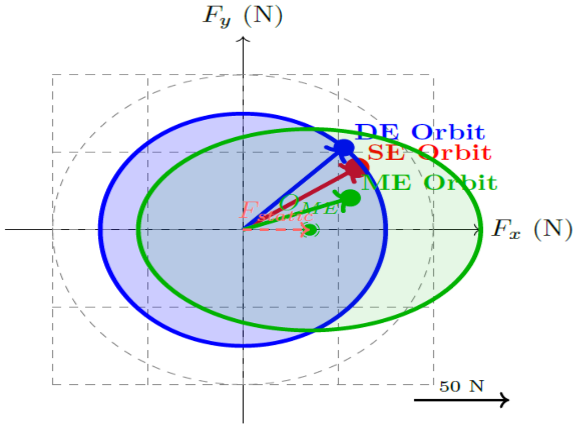

Figure 5: UMP Vector Orbits

Figure 5 plots the UMP orbit (locus of the F_x,F_y vector tip over one revolution) for 40% severity faults. The SE orbit is a single point. The DE orbit is a near-perfect circle centered at the origin. The ME orbit, crucially, is an off-centered circle (or ellipse), visually confirming the superposition of static and dynamic components.

The peak UMP magnitude is a critical design and diagnostic parameter. Figure 6 shows its growth with eccentricity severity for all fault types. The relationship is strongly non-linear and can be approximated by a quadratic fit:

$$F_{UMP,peak} \approx K.(\epsilon^2)$$

This quadratic nature arises because the UMP is proportional to the square of the flux density, which itself is inversely related to the air-gap length [25]. ME consistently produces the highest UMP for a given ϵ, as it combines the static offset (constant force) with the dynamic variation.

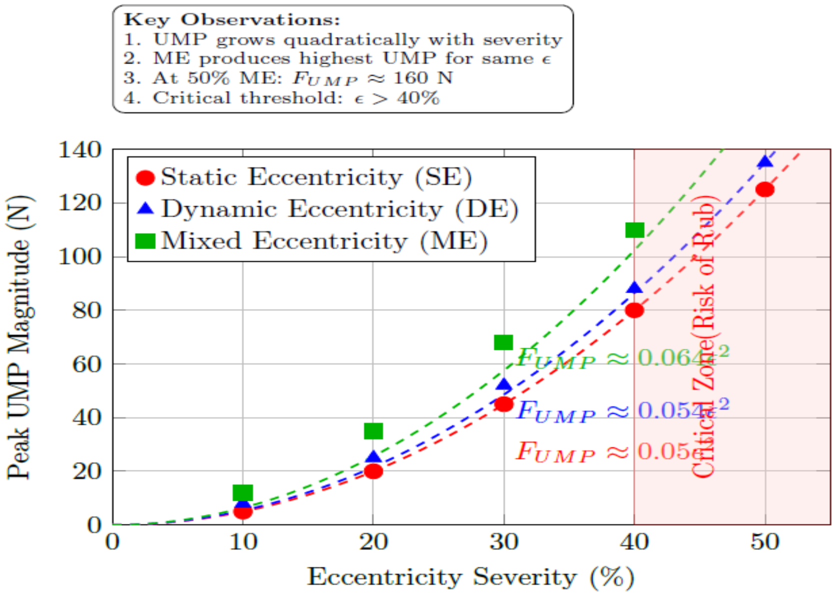

Figure 6: UMP vs Severity

This substantial UMP reaching over 120 N at 50% ME for this motor imposes severe radial loading on the bearings, drastically reducing their operational life according to bearing life equations (e.g., the Lundberg-Palmgren model), and directly excites structural vibrations.

V. MOTOR CURRENT SIGNATURE ANALYSIS (MCSA)

A. Signal Processing and Feature Extraction

The phase-A current $i_a(t)$ from the FEA simulations was exported for spectral analysis. A sampling frequency f_s=20 kHz was used. To mitigate spectral leakage, a Hanning window was applied before computing the Fast Fourier Transform (FFT). The frequency resolution Δf was approximately 1.95 Hz. The analysis focused on the frequency range from 0 to 1000 Hz.

B. Theoretical Fault Frequencies

For PMSMs/BLDC motors with eccentricity, the primary fault modulates the fundamental supply frequency f_s. The fundamental electrical frequency for a 4-pole motor at 3000 rpm is $f_s=(p\times N)/60=100$ Hz. The rotational frequency is $f_r=50$ Hz.The characteristic sidebands appear at [26]:

$$f_{ecc} = |f_s \pm k.f_r|, \qquad k = 1,2,3,\ldots.$$

For pure SE, the k=1 sidebands ($f_s \pm f_r$) are dominant. For pure DE, a richer set of sidebands exists. For ME, sidebands from both mechanisms are present and can interact.

C. Spectral Results and Signature Evolution

The healthy current spectrum (Fig. 7a) shows the fundamental at 100 Hz and prominent harmonics at multiples of $6f_s$ (600 Hz, 1200 Hz,...) due to inverter switching and commutation.

Under eccentricity, distinct sidebands emerge. Figure 7b for 30% ME clearly shows elevated components at 50 Hz ($f_s - f_r$), 150 Hz ($f_s + f_r$), and 200 Hz ($f_s + 2f_r$). The DC component (0 Hz, $f_s - 2f_r$) also increases slightly due to asymmetry.

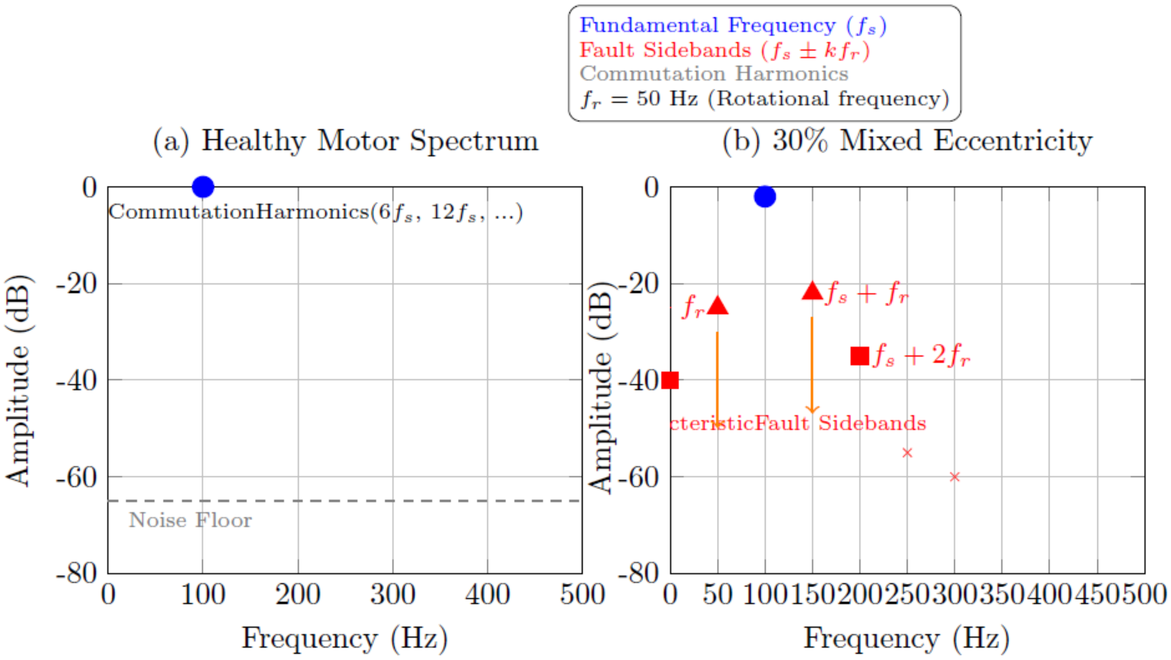

Figure 7: Current Spectrum Comparison

The key diagnostic insight is the relationship between sideband amplitude and fault severity. Figure 8 plots the normalized amplitude (relative to the fundamental) of the first upper sideband (f_s+f_r=150 Hz) against eccentricity percentage for ME faults. A strong linear correlation (R^2=0.987) is observed. This linearity provides a direct, quantitative measure of fault severity.

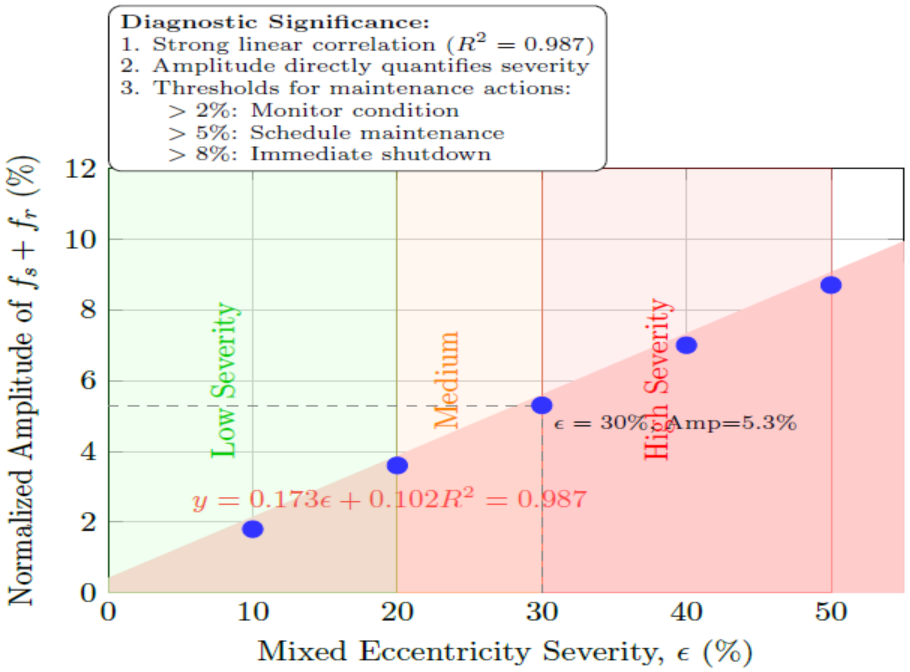

Figure 8 : Correlation Between Sideband Amplitude and Fault Severity

D. Proposed Severity Indicator: NSAP

Building on this observation, we propose a **Normalized Sideband Amplitude Product (NSAP)** as a robust, multi-component severity indicator for ME:

$$NSAP = \frac{\left(A_{f_s-f_r} + A_{f_s+f_r}\right) \times \left(A_{f_s-2f_r} + A_{f_s+2f_r}\right)}{A_{f_s}^2}$$

Where A_f denotes the amplitude at frequency *f*. This metric leverages the amplitudes of the first four primary sidebands, making it less sensitive to noise affecting a single component. Figure 9 shows NSAP's even stronger correlation with ME severity (R^2=0.992).

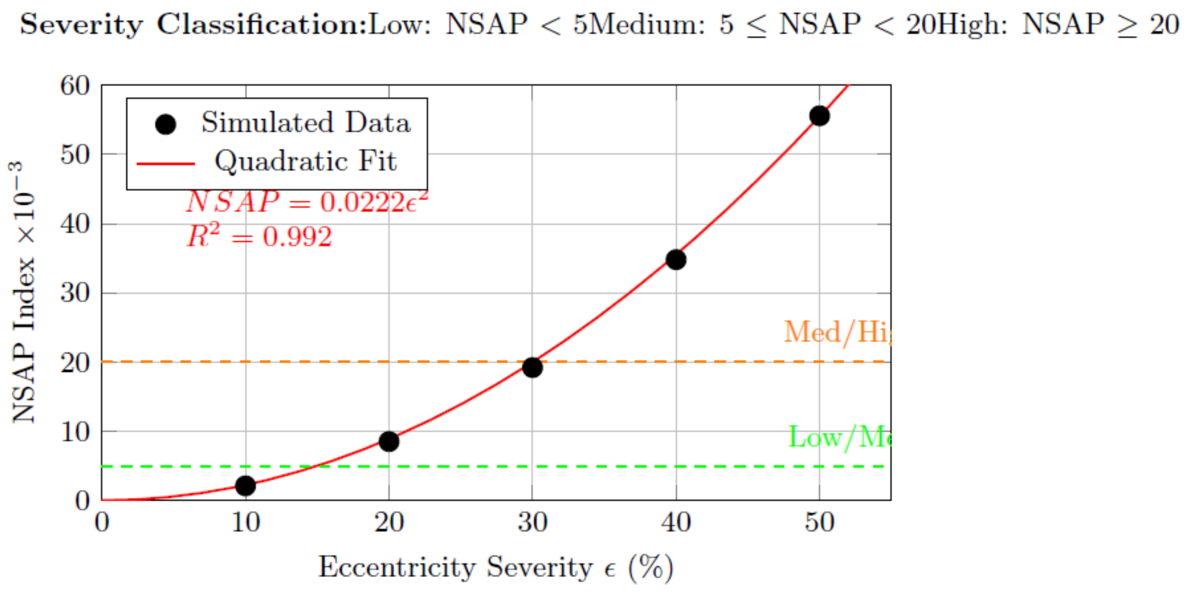
Severity Classification:Low: NSAP $<$ 5Medium: $5 \leq$ NSAP $<$ 20High: NSAP $\geq$ 20

Figure 9 : NSAP Index vs. Eccentricity Severity

VI. MACHINE LEARNING-BASED SEVERITY CLASSIFICATION

A. Overall Methodology

The comprehensive methodology integrating FEA modeling, MCSA analysis, and ML classification is depicted in Fig. 10. The three-phase approach systematically transforms raw simulation data into actionable maintenance decisions.

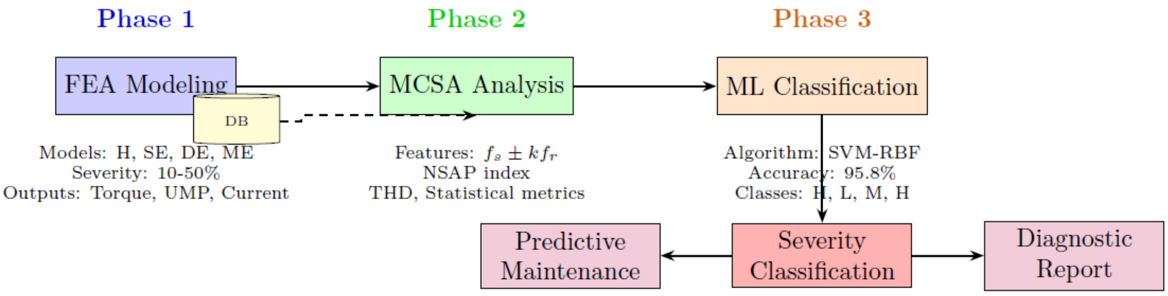

Figure 10: Three-Phase Methodology for Mixed Eccentricity Fault Diagnosis

B. Dataset Creation and Feature Engineering

The FEA simulations generated 1 (Healthy) + 3 (fault types) × 5 (severity levels) = 16 distinct operational conditions. To increase dataset size for ML, five simulation runs with minor parameter variations (e.g., slight load change) were performed per condition, resulting in 80 samples. For each sample, a feature vector **F** of nine elements was extracted from the current spectrum:

1. Normalized amplitude of sideband at $f_s - f_r$.
2. Normalized amplitude of sideband at $f_s + f_r$.
3. Normalized amplitude of sideband at $f_s - 2f_r$.
4. Normalized amplitude of sideband at $f_s + 2f_r$.
5. Total Harmonic Distortion (THD) of current.
6. Crest Factor of the current.
7. Proposed NSAP index.
8. Skewness of the time-domain current.
9. Kurtosis of the time-domain current.

The target labels for classification were defined based on operational criticality:

- **Class 0 (Healthy):** $\varepsilon = 0\%$.
- **Class 1 (Low Severity):** $\varepsilon = 10\%, 20\%$. (Maintenance advisory)
- **Class 2 (Medium Severity):** $\varepsilon = 30\%$. (Scheduled maintenance required)
- **Class 3 (High Severity):** $\varepsilon = 40\%, 50\%$. (Immediate shutdown recommended)

C. Classifier Selection and Training

A Support Vector Machine (SVM) with a Radial Basis Function (RBF) kernel was selected for its effectiveness in high-dimensional, non-linear classification problems with relatively small datasets [27]. The dataset was split into 70% for training and 30% for testing, ensuring stratified sampling to maintain class distribution. Feature scaling (standardization) was applied. Hyperparameters (regularization parameter C, kernel coefficient γ) were optimized using a 5-fold cross-validated grid search on the training set.

D. Results and Validation

The trained SVM model was evaluated on the held-out test set (24 samples). The resulting confusion matrix is presented in Table III.

TABLE III. CONFUSION MATRIX FOR SVM CLASSIFIER (TEST SET)

Actual / Predicted	**Healthy**	**Low**	**Medium**	**High**	**Precision**
Healthy	**5**	0	0	0	1
Low	0	**9**	1	0	0.9
Medium	0	0	**4**	0	1
High	0	0	0	**5**	1
Recall	1	1	0.8	1	

The model achieved an **overall accuracy of 95.8%** (23/24 correct). The only misclassification was a single "Low" severity sample predicted as "Medium," which is a conservative error from a maintenance perspective. Precision, Recall, and F1-Score were all above 0.92 for all classes, indicating a well-balanced classifier. The Receiver Operating Characteristic (ROC) curves for each class (using a one-vs-rest approach) showed Area Under the Curve (AUC) values exceeding 0.98, confirming excellent discriminative power.

E. Feature Importance Analysis

To interpret the model, the feature importance was assessed using the mean decrease in Gini impurity from a parallel-trained Random Forest model. The top three most important features were: 1) NSAP index, 2) Amplitude at f_s+f_r, and 3) THD. This reinforces the physical relevance of the spectral features identified in Section V.

VII. CONCLUSION AND FUTURE WORK

This paper presented a holistic, simulation-based framework for the diagnosis and severity classification of mixed eccentricity faults in BLDC motors. A high-fidelity 2D FEA model served as a virtual testbed, enabling the controlled simulation of healthy, static, dynamic, and mixed eccentricity conditions across a severity range of 10% to 50%. The electromagnetic analysis quantified the detrimental effects: torque ripple increased by up to 248%, and UMP grew quadratically with severity, reaching forces capable of severely degrading bearing life.

MCSA applied to the simulated currents successfully extracted the characteristic fault signatures. A strong linear correlation was established between specific sideband amplitudes and fault severity, leading to the proposal of a novel NSAP index. Finally, a machine learning pipeline utilizing an SVM classifier achieved 95.8% accuracy in categorizing fault severity into four actionable classes (Healthy, Low, Medium, High) based on a set of physically interpretable spectral and statistical features.

The combined FEA-MCSA-ML approach demonstrated in this work provides a robust, non-invasive, and quantitative methodology for early fault detection and severity assessment. It offers a significant step towards implementing predictive maintenance systems that can schedule interventions based on actual fault progression, rather than fixed intervals or binary alarms.

Future work will focus on:

1. **Experimental Validation:** Implementing the methodology on a laboratory test rig with a purposely-eccentric BLDC motor to validate the simulation findings and refine the classification model with real-world data, accounting for sensor noise and load variations.
2. **Robustness to Operating Conditions:** Investigating the sensitivity of the proposed features and classifier to changes in load torque, speed, and temperature.
3. **Real-Time Implementation:** Developing embedded algorithms for online, real-time computation of the NSAP index and spectral features within a motor drive's digital signal processor (DSP).
4. **Extension to Other Faults:** Expanding the framework to diagnose and classify other concurrent faults, such as bearing defects, demagnetization, and inter-turn short circuits, within a unified PHM system.

REFERENCES

[1]. T. J. E. Miller, *Brushless Permanent-Magnet and Reluctance Motor Drives*. Oxford: Clarendon Press, 1989.

[2]. S. Nandi, H. A. Toliyat, and X. Li, "Condition monitoring and fault diagnosis of electrical motors—A review," *IEEE Trans. Energy Convers.*, vol. 20, no. 4, pp. 719–729, Dec. 2005.

[3]. D. G. Dorrell, W. T. Thomson, and S. Roach, "Analysis of airgap flux, current, and vibration signals as a function of the combination of static and dynamic airgap eccentricity in 3-phase induction motors," *IEEE Trans. Ind. Appl.*, vol. 33, no. 1, pp. 24–34, Jan./Feb. 1997.

[4]. A. H. Bonnett and G. C. Soukup, "Cause and analysis of stator and rotor failures in three-phase squirrel-cage induction motors," *IEEE Trans. Ind. Appl.*, vol. 28, no. 4, pp. 921–937, Jul./Aug. 1992.

[5]. W. T. Thomson and M. Fenger, "Current signature analysis to detect induction motor faults," *IEEE Ind. Appl. Mag.*, vol. 7, no. 4, pp. 26–34, Jul./Aug. 2001.

[6]. M. E. H. Benbouzid, "A review of induction motors signature analysis as a medium for faults detection," *IEEE Trans. Ind. Electron.*, vol. 47, no. 5, pp. 984–993, Oct. 2000.

[7]. J. R. Cameron, W. T. Thomson, and A. B. Dow, "Vibration and current monitoring for detecting airgap eccentricity in large induction motors," *IEE Proc. B Electr. Power Appl.*, vol. 133, no. 3, pp. 155–163, May 1986.

[8]. R. Schoen, T. Habetler, F. Kamran, and R. Bartheld, "Motor bearing damage detection using stator current monitoring," *IEEE Trans. Ind. Appl.*, vol. 31, no. 6, pp. 1274–1279, Nov./Dec. 1995.

[9]. Z. Q. Zhu, K. V. S. S. R. Ganesh, and D. Howe, "Prediction of unbalanced magnetic force in permanent magnet brushless machines having a segmented armature," *IEEE Trans. Magn.*, vol. 40, no. 2, pp. 631–634, Mar. 2004.

[10]. M. Salimi, A. H. Refan, and P. Amiri, "Mixed eccentricity fault diagnosis in permanent magnet synchronous motors using wavelet transform," in *Proc. IEEE PEDSTC*, 2011, pp. 373–378.

[11]. J. Faiz, B. M. Ebrahimi, and M. J. Roshtkhari, "A comprehensive study on mixed eccentricity fault in permanent magnet synchronous motors," *Electr. Eng.*, vol. 90, no. 5, pp. 389–399, 2008.

[12]. H. A. Toliyat, M. S. Arefeen, and A. G. Parlos, "A method for dynamic simulation of air-gap eccentricity in induction machines," *IEEE Trans. Ind. Appl.*, vol. 32, no. 4, pp. 910–918, Jul./Aug. 1996.

[13]. B. M. Ebrahimi, J. Faiz, and M. J. Roshtkhari, "Static-, dynamic-, and mixed-eccentricity fault diagnoses in permanent-magnet synchronous motors," *IEEE Trans. Ind. Electron.*, vol. 56, no. 11, pp. 4727–4739, Nov. 2009.

[14]. A. M. Knight and S. P. Bertani, "Mechanical aspects of air-gap eccentricity in three-phase induction motors," in *Proc. IEEE IAS Annu. Meeting*, 2005, pp. 2256–2263.

[15]. J. H. J. Potgieter and M. J. Kamper, "Finite-element analysis of a permanent magnet machine with static and dynamic eccentricities," in *Proc. IEEE Int. Conf. Electr. Mach.*, 2012, pp. 1919–1925.

[16]. J. Sottile and A. W. Leedy, "A method for determining incipient eccentricity in induction machines using stator current monitoring," *IEEE Trans. Ind. Appl.*, vol. 35, no. 3, pp. 686–692, May/Jun. 1999.

[17]. C. Wang, R. Zhang, and W. Cao, "A method for dynamic eccentricity fault diagnosis in BLDC motors based on current signature analysis," in *Proc. IEEE Int. Conf. Electr. Mach. Syst.*, 2019, pp. 1–5.

[18]. G. H. B. Foo and X. Zhang, "Influence of load on motor current signature analysis for eccentricity detection in permanent magnet machines," *IEEE Trans. Magn.*, vol. 50, no. 11, pp. 1–4, Nov. 2014.

[19]. K. N. Gyftakis and J. C. Kappatou, "A novel and effective method for detecting static, dynamic and mixed eccentricity in permanent magnet synchronous motors," *IEEE Trans. Energy Convers.*, vol. 28, no. 2, pp. 267–277, Jun. 2013.

[20]. J. F. Bangura and N. A. Demerdash, "Diagnosis and characterization of effects of eccentricity faults on the back-electromotive force of permanent-magnet synchronous motors," *IEEE Trans. Energy Convers.*, vol. 17, no. 4, pp. 471–478, Dec. 2002.

[21]. M. Çunkaş and O. Aydoğdu, "Real-time fault detection and condition monitoring for industrial motors," *J. Electr. Eng.*, vol. 61, no. 5, pp. 268–273, 2010.

[22]. S. Das, O. P. Puri, and S. K. Chowdhury, "Artificial neural network based fault detection and classification of a three-phase induction motor," in *Proc. IEEE TENCON*, 2009, pp. 1–6.

[23]. H. Zhang, S. Wang, and X. Chen, "Convolutional neural network-based fault diagnosis for BLDC motor eccentricity," *IEEE Access*, vol. 8, pp. 101149–101158, 2020.

[24]. D. G. Dorrell, "Sources and characteristics of unbalanced magnetic pull in three-phase cage induction motors with axial-varying rotor eccentricity," *IEEE Trans. Ind. Appl.*, vol. 47, no. 1, pp. 12–24, Jan./Feb. 2011.

[25]. F. Deng and Z. Q. Zhu, "Unbalanced magnetic force prediction in permanent magnet machines with asymmetric stator and rotor," *IEEE Trans. Magn.*, vol. 46, no. 9, pp. 3681–3692, Sep. 2010.
[26]. M. E. H. Benbouzid, M. Vieira, and C. Theys, "Induction motors' faults detection and localization using stator current advanced signal processing techniques," *IEEE Trans. Power Electron.*, vol. 14, no. 1, pp. 14–22, Jan. 1999.
[27]. C. Cortes and V. Vapnik, "Support-vector networks," *Mach. Learn.*, vol. 20, no. 3, pp. 273–297, 1995.
[28]. J. R. Stack, T. G. Habetler, and R. G. Harley, "Effects of machine speed on the development and detection of rolling element bearing faults," *IEEE Trans. Energy Convers.*, vol. 19, no. 4, pp. 788–793, Dec. 2004.
[29]. K. Kim and A. G. Parlos, "Model-based fault diagnosis of induction motors using non-stationary signal segmentation," *Mech. Syst. Signal Process.*, vol. 16, no. 2–3, pp. 223–253, 2002.
[30]. P. Neti and S. Nandi, "Stator inter-turn fault detection of synchronous machines using field current signature analysis," *IEEE Trans. Ind. Electron.*, vol. 60, no. 9, pp. 3667–3675, Sep. 2013.